Residual Flow and Boundary Shear Stress in the Turbulent Bottom Layer Beneath Waves

B. JOHNS

Department of Meteorology, University of Reading, Reading, England

(Manuscript received 28 February 1977, in revised form 6 May 1977)

ABSTRACT

A model is considered of the turbulent bottom boundary layer beneath waves. Closure is effected at the level of the turbulent energy equation and numerical solutions are obtained by a combination of finite-difference methods and a pseudo-spectral technique. These solutions are used to evaluate the induced streaming motion and the boundary shear stress. An expression is derived for the friction coefficient in terms of the bottom roughness and this is found to agree with values reported in experimental studies.

1. Introduction

The mechanics of the bottom boundary layer beneath waves is of importance in theories relating to sediment movement (Carter *et al.*, 1973) and the generation of longshore currents (Longuet-Higgins, 1970). In field conditions, the flow in this layer may be turbulent even over smooth beds, and Collins (1963) has determined a parameter whose value indicates the type of flow regime that exists. This parameter is a Reynolds number defined by

$$R_\delta = \frac{u_\infty \delta}{\nu},$$

where u_∞ is the amplitude of the orbital wave velocity just beyond the layer, $\delta = (2\nu/\sigma)^{\frac{1}{2}}$, ν is the kinematic viscosity of the fluid and σ the radian frequency of the waves. Collins' experimental results indicate that for $R_\delta < 160$ the flow is laminar, while for $R_\delta > 160$ the flow in the boundary layer becomes intermittently turbulent. For typical field data in which $u_\infty = 30$ cm s^{-1}, $\sigma = 1$ rad s^{-1}, $\nu = 1.4 \times 10^{-2}$ cm^2 s^{-1} it follows that $R_\delta \approx 360$ and the boundary layer flow may therefore be expected to be fully turbulent. A determination of induced streaming motions and the boundary shear stress must then take account of this fact.

For laminar flow conditions it is well known (Longuet-Higgins, 1953) that a progressive wave leads to a maximum streaming velocity given by

$$\langle u \rangle / u_\infty = 0.75\alpha + O(\alpha^3), \quad \alpha = k u_\infty / \sigma, \qquad (1.1)$$

where k is the radian wavenumber of the driving wave motion. For $R_\delta < 160$, this result has received experimental confirmation by Collins (1963). If, however, $R_\delta > 160$, the trend in Collins' results suggests a qualitatively similar streaming phenomenon which appears to have a reduced magnitude compared with (1.1). A treatment of the induced streaming in a turbulent shear wave boundary layer has been given by Longuet-Higgins in a supplement to Russell and Osorio (1958) and Johns (1970). In these studies, the kinematical viscosity ν (appearing in the laminar formulation) is replaced by a phase-independent coefficient of eddy viscosity which is a function of the distance above the solid boundary. The maximum induced streaming velocity is then found to be independent of the eddy viscosity and to be identical to (1.1). These results appear to be contradicted by Collins' experimental study and doubt is therefore cast on the adequacy of the proposed model.

As well as the relevance of induced streaming to sediment movement by waves, a knowledge of the boundary stress is important in estimating sediment entrainment. Additionally, an adequate representation of the boundary shear stress is required in theories relating to the generation of longshore currents by obliquely incident sea waves. In this connection, the work of Longuet-Higgins (1970) may be mentioned where the choice of a bottom friction coefficient plays a crucial role in the application of the theory.

In the present work, a relatively refined model of a fully turbulent wave boundary layer is used to determine the induced streaming effects and the boundary shear stress. The induced streaming is found to be compatible with the trend suggested by Collins' experimental results. The numerical evaluations of the boundary shear stress are used to determine a friction coefficient and its variation with bottom roughness. The value of this coefficient is found to compare well with that reported in experimental studies.

2. Formulation of model

Coordinates are chosen in which x measures the distance along a plane horizontal boundary and y the distance above the boundary. The equations for the balance of momentum and turbulent energy density in the layer adjacent to $y=0$ then have the form

$$\frac{\partial \bar{u}}{\partial t}+\frac{\partial}{\partial x}\bar{u}^2+\frac{\partial}{\partial y}\bar{u}\bar{v}=\frac{\partial U}{\partial t}+U\frac{\partial U}{\partial x}+\frac{\partial}{\partial y}(-\overline{u'v'}), \quad (2.1)$$

$$\frac{\partial \bar{E}}{\partial t}+\frac{\partial}{\partial x}(\bar{u}\bar{E})+\frac{\partial}{\partial y}(\bar{v}\bar{E})=(-\overline{u'v'})\frac{\partial \bar{u}}{\partial y}+\frac{\partial}{\partial y}\left[-\overline{v'\left(\frac{p'}{\rho}+E'\right)}\right]-\epsilon. \quad (2.2)$$

In these equations, the overbar denotes a Reynolds average and the prime a turbulent departure from that average. The velocity U in the turbulent-free mainstream flow is given by

$$U=u_\infty \cos(kx-\sigma t). \quad (2.3)$$

The quantity ϵ specifies the rate of dissipation of turbulent energy in the system.

Closure hypotheses for Eqs. (2.1) and (2.2) are based upon those used by Launder and Spalding (1972):

$$\left.\begin{aligned}-\overline{u'v'}&=K\frac{\partial \bar{u}}{\partial y}\\ -\overline{v'\left(\frac{p'}{\rho}+E'\right)}&=K\frac{\partial \bar{E}}{\partial y}\end{aligned}\right\}. \quad (2.4)$$

The diffusion coefficient K is therefore assumed to be the same for both momentum and energy fluxes. As a first step in modeling the oscillatory turbulent boundary layer, this frequently used assumption appears preferable to the use of different coefficients for the two processes. Using dimensional reasoning, K and ϵ are then expressed in the form

$$\left.\begin{aligned}K&=l\bar{E}^{\frac{1}{2}}\\ \epsilon&=\frac{\bar{E}^{\frac{3}{2}}}{l'}\end{aligned}\right\}, \quad (2.5)$$

where l and l' are appropriate length scales.

By considering the balance of the turbulent energy density adjacent to $y=0$, where production tends to equal the dissipation, it may be shown that the formulation reduces to a mixing length hypothesis provided that

$$l\sim c^{\frac{1}{4}}\kappa y, \quad l'\sim c^{-\frac{3}{4}}\kappa y, \quad \text{as} \quad y\to 0. \quad (2.6)$$

The quantity c is an experimentally determined constant taken to be 0.08 while κ is von Kármán's constant 0.4. Details of this reduction are given by Launder and Spalding (1972). In the present work the asymptotic values (2.6) are assumed to apply for all values of y within the boundary layer. It may, perhaps, be more realistic to suppose that l and l' approach constant values toward the edge of the boundary or, alternatively, the length scale may be made the object of a similarity hypothesis of the type used by Weatherly (1975) in an investigation into time-dependent flow in a turbulent Ekman layer. However, it seems unlikely that conditions near $y=0$ will be strongly influenced by our assumption.

Introducing these results into (2.1) and (2.2), the Reynolds-averaged flow conditions in the boundary layer are determined from

$$\frac{\partial \bar{u}}{\partial t}+\frac{\partial}{\partial x}\bar{u}^2+\frac{\partial}{\partial y}\bar{u}\bar{v}=\frac{\partial U}{\partial t}+U\frac{\partial U}{\partial x}+\frac{\partial}{\partial y}\left(K\frac{\partial \bar{u}}{\partial y}\right), \quad (2.7)$$

$$\frac{\partial \bar{E}}{\partial t}+\frac{\partial}{\partial x}(\bar{u}\bar{E})+\frac{\partial}{\partial y}(\bar{v}\bar{E})=K\left(\frac{\partial \bar{u}}{\partial y}\right)^2+\frac{\partial}{\partial y}\left(K\frac{\partial \bar{E}}{\partial y}\right)-\epsilon, \quad (2.8)$$

where

$$\left.\begin{aligned}K&=c^{\frac{1}{4}}\kappa y\bar{E}^{\frac{1}{2}}\\ \epsilon&=\frac{c^{\frac{3}{4}}\bar{E}^{\frac{3}{2}}}{\kappa y}\end{aligned}\right\}. \quad (2.9)$$

Eqs. (2.7)–(2.9) evidently have a singular behavior at $y=0$ and the lower boundary conditions must therefore be applied at some level $y=y_0$. Close to the lower boundary ($y\lesssim y_0$) we follow Jonsson and Carlsen (1976), who found evidence of a logarithmic profile beneath waves, and prescribe a variation in the Reynolds-averaged velocity given by

$$\bar{u}=V(x,t)\ln(y/y_*), \quad (2.10)$$

where y_* is the roughness length of the underlying elements. Accordingly,

$$\frac{\partial \bar{u}}{\partial y}=\frac{\bar{u}}{y\ln(y/y_*)}, \quad (2.11)$$

and we take

$$y_0\ln(y_0/y_*)\frac{\partial \bar{u}}{\partial y}=\bar{u} \quad \text{at} \quad y=y_0. \quad (2.12)$$

The corresponding value of $\bar{v}$ may be deduced by consideration of the equation of continuity in the boundary layer, namely

$$\frac{\partial \bar{u}}{\partial x}+\frac{\partial \bar{v}}{\partial y}=0. \quad (2.13)$$

Insertion of (2.10) into (2.13) is readily found to yield

$$\bar{v}\ln(y_0/y_*)=[y_0\ln(y_0/y_*)+y_0-y_*]\frac{\partial \bar{u}}{\partial x} \quad \text{at} \quad y=y_0. \quad (2.14)$$

An appropriate boundary condition on $\bar{E}$ at $y=y_0$ may be derived by using the equation expressing a balance between the production and dissipation of averaged turbulent energy, i.e.,

$$K\left(\frac{\partial \bar{u}}{\partial y}\right)^2=\epsilon. \tag{2.15}$$

Substituting in (2.15) from (2.9) we find that

$$\bar{E}=(\kappa y)^2 c^{-\frac{1}{2}}\left(\frac{\partial \bar{u}}{\partial y}\right)^2 \quad \text{as} \quad y\to 0, \tag{2.16}$$

and on application of (2.10) it follows that

$$\bar{E}=\kappa^2 c^{-\frac{1}{2}}V^2 \quad \text{for} \quad y_*\leqslant y\leqslant y_0. \tag{2.17}$$

An appropriate condition to be satisfied by $\bar{E}$ is therefore

$$\frac{\partial \bar{E}}{\partial y}=0 \quad \text{at} \quad y=y_0. \tag{2.18}$$

Naturally, in the subsequent evaluations, it will be necessary to determine a suitable value of y_0 to be used in this specification.

Appropriate boundary conditions to be applied at the outer edge of the boundary layer present no problem. Denoting this level by $y=y_1$, it is necessary for the boundary layer flow to merge into the imposed oscillatory mainstream flow and so we take

$$\bar{u}=u_\infty \cos(kx-\sigma t) \quad \text{at} \quad y=y_1. \tag{2.19}$$

Additionally, it is prescribed that there is no flux of turbulent energy across the outer edge of the layer thus leading to

$$\frac{\partial \bar{E}}{\partial y}=0 \quad \text{at} \quad y=y_1. \tag{2.20}$$

In order to obtain numerical results independent of y_1, it will be necessary to select a value for y_1 which is such that (2.19) and (2.20) are effectively satisfied for $y<y_1$.

3. Nondimensionalization and numerical solution

For computational purposes, it is convenient to nondimensionalize the equations in Section (2) by writing

$$\left.\begin{aligned}\hat{x}&=kx\\ \hat{y}&=\frac{\sigma}{u_\infty}(y-y_0)\\ \hat{t}&=\sigma t\end{aligned}\right\}, \tag{3.1}$$

$$\left.\begin{aligned}\bar{u}&=u_\infty \hat{u}\\ \bar{v}&=\frac{ku_\infty^2}{\sigma}\hat{v}\\ K&=\frac{u_\infty^2}{\sigma}\hat{K}\\ \bar{E}&=u_\infty^2\hat{E}\\ \epsilon&=u_\infty^2\sigma\hat{\epsilon}\end{aligned}\right\}. \tag{3.2}$$

Eqs. (2.7), (2.8) and (2.13) then become

$$\frac{\partial \hat{u}}{\partial \hat{t}}+\alpha\left(\frac{\partial}{\partial \hat{x}}\hat{u}^2+\frac{\partial}{\partial \hat{y}}\hat{u}\hat{v}\right)=\sin(\hat{x}-\hat{t})-\tfrac{1}{2}\alpha\sin 2(\hat{x}-\hat{t})+\frac{\partial}{\partial \hat{y}}\left(\hat{K}\frac{\partial \hat{u}}{\partial \hat{y}}\right), \tag{3.3}$$

$$\frac{\partial \hat{E}}{\partial t}+\alpha\left(\frac{\partial}{\partial \hat{x}}(\hat{u}\hat{E})+\frac{\partial}{\partial \hat{y}}(\hat{v}\hat{E})\right)=\hat{K}\left(\frac{\partial \hat{u}}{\partial \hat{y}}\right)^2+\frac{\partial}{\partial \hat{y}}\left(\hat{K}\frac{\partial \hat{E}}{\partial \hat{y}}\right)-\hat{\epsilon}, \tag{3.4}$$

$$\frac{\partial \hat{u}}{\partial \hat{x}}+\frac{\partial \hat{v}}{\partial \hat{y}}=0. \tag{3.5}$$

In these equations,

$$\alpha=\frac{ku_\infty}{\sigma} \tag{3.6}$$

$$\left.\begin{aligned}\hat{K}&=c^{\frac{1}{4}}\kappa(\hat{y}+\hat{y}_0)\hat{E}^{\frac{1}{2}}\\ \hat{\epsilon}&=\frac{c^{\frac{3}{4}}\hat{E}^{\frac{3}{2}}}{\kappa(\hat{y}+\hat{y}_0)}\\ \hat{y}_0&=\frac{\sigma y_0}{u_\infty}\end{aligned}\right\}. \tag{3.7}$$

The accompanying boundary conditions are

$$\left.\begin{aligned}\hat{y}_0\ln(\hat{y}_0/\hat{y}_*)\frac{\partial \hat{u}}{\partial \hat{y}}&=\hat{u}\\ \ln(\hat{y}/\hat{y}_*)\hat{v}&=[\hat{y}_0\ln(\hat{y}_0/\hat{y}_*)+\hat{y}_0-\hat{y}_*]\frac{\partial \hat{u}}{\partial x}\\ \frac{\partial \hat{E}}{\partial \hat{y}}&=0\end{aligned}\right\} \text{ at } \hat{y}=0, \tag{3.8}$$

$$\left.\begin{aligned}\hat{u}&=\cos(\hat{x}-\hat{t})\\ \frac{\partial \hat{E}}{\partial \hat{y}}&=0\end{aligned}\right\} \text{ at } \hat{y}=\hat{y}_1, \tag{3.9}$$

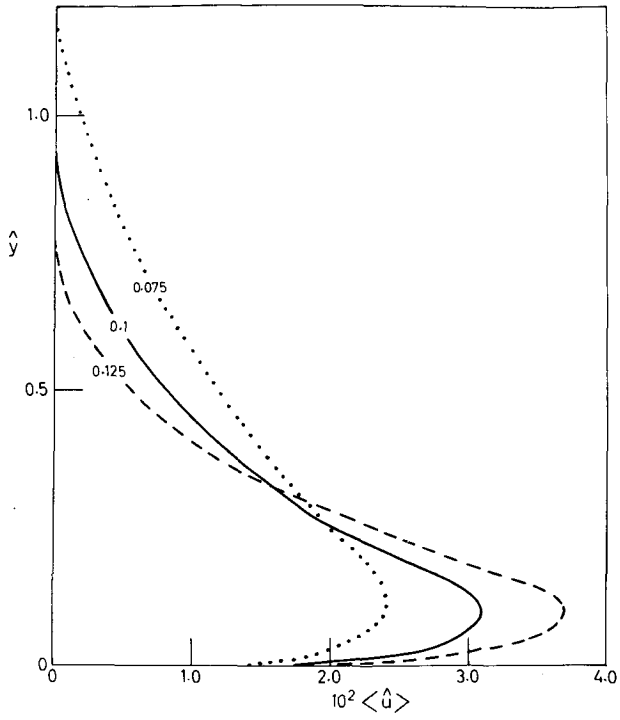

FIG. 1. Boundary layer profile of induced streaming: $\alpha=0.075$, 0.1, 0.125; $\alpha\hat{y}_*=3\times10^{-4}$.

where

$$\hat{y}_*=(\sigma/u_\infty)y_*, \quad \hat{y}_1=(\sigma/u_\infty)(y_1-y_0). \tag{3.10}$$

A method of numerical solution of the foregoing system of equations is applied in which a stretched finite-difference grid is used in the $\hat{y}$ direction. This permits a high resolution near $\hat{y}=0$ relative to that near $\hat{y}=\hat{y}_1$ and thus leads to an accurate representation of the high shears encountered near the boundary. The time variable is replaced by a discrete sequence of time-instants. A novelty of the method consists of representing the variation with $\hat{x}$ by a Fourier method in which we write

$$\left.\begin{aligned}\hat{u}(\hat{x},\hat{y},\hat{t})&=\sum_{p=-2M}^{2M}C_p(\hat{y},\hat{t})e^{ip\hat{x}}, \quad i^2=-1\\ \hat{E}(\hat{x},\hat{y},\hat{t})&=\sum_{p=-2M}^{2M}D_p(\hat{y},\hat{t})e^{ip\hat{x}}\end{aligned}\right\}. \tag{3.11}$$

The numerical solution is then obtained by a pseudo-spectral technique in which Eqs. (3.3)–(3.5) are treated as an initial value problem, the initial state being specified as one of no motion. The developing numerical response satisfies the boundary conditions (3.8) and (3.9) and, after a sufficient period of integration, becomes a purely oscillatory function of $\hat{t}$, reproducing itself from one cycle of integration to the next. A similar initial value approach was used by Weatherly (1975) in the Ekman layer problem, but without the inclusion of the nonlinear advective terms. In our procedure, a fairly standard "Fourier chopping" method is applied to avoid mid-representation of the nonlinear terms through aliasing. Effectively, this means that there will be a total of M significant Fourier components in (3.11) since, prior to the evaluation of a nonlinear product, the Fourier representation is halved in order to suppress the development of nonresolvable components in a quadratic interaction. The nonlinear products are evaluated in grid-point space, the switching between physical and wavenumber space being achieved by a fast Fourier transform procedure.

4. Numerical evaluation

A series of numerical experiments has been performed to determine the dependence of the solution of the equations in Section 3 on the parameters α and $\hat{y}_*$. We first consider $0.075\leqslant\alpha\leqslant0.125$, $\alpha\hat{y}_*=3\times10^{-4}$, $\alpha\hat{y}_0=2\times10^{-3}$ and $\alpha\hat{y}_1=0.1$. The selection of a smaller value for $\hat{y}_0$ is, unfortunately, found to lead to numerical problems related to the increasing influence of the singularity in (3.3) and (3.4). With these values, and field data given by $h=1$ m, $\sigma=1$ rad s^{-1} and $a=10$ cm, we find that $\alpha=0.1$, $u_\infty\approx31$ cm s^{-1}, $y_*\approx0.9$ mm, $y_1\approx31$ cm and $y_0\approx0.63$ cm.

With $M=3$, the response (3.11) is found to become effectively oscillatory after 30 cycles of integration (when $\hat{t}=60\pi$) at which time we can write the oscillatory solution in the form

$$\hat{u}=\langle\hat{u}(\hat{y})\rangle+\sum_{p=1}^{3}[A_p\cos p\chi+B_p\sin p\chi], \tag{4.1}$$

$$\hat{E}=\langle\hat{E}(\hat{y})\rangle+\sum_{p=1}^{3}[G_p\cos p\chi+H_p\sin p\chi], \tag{4.2}$$

where

$$\chi=\hat{x}-\hat{t}. \tag{4.3}$$

Characteristic values of $\hat{K}$ at $\hat{y}=0$ are found to be of order 5×10^{-4} and the condition for a fully turbulent layer ($K\gg\nu$) is found to lead to the requirement $\hat{K}\gg2/\mathrm{R}_\delta^2$ which, with $\mathrm{R}_\delta=360$, is clearly fulfilled. Turbulent velocity fluctuations are of order $\bar{E}^{\frac{1}{2}}$ and, near $\hat{y}=0$, have a characteristic value $0.1\,u_\infty$.

In Fig. 1 we give the variation of the streaming velocity $\langle u\rangle$ through the boundary layer for $\alpha=0.075$, 0.1 and 0.125. The streaming velocity reaches a maximum at a level within the boundary layer that is independent of α. Its value then satisfies

$$\langle\hat{u}\rangle_{\max}=0.30\alpha+\mathrm{O}(\alpha^3), \tag{4.4}$$

and reduces to zero through an outer layer that thickens as $\alpha\to0$. It will also be noted that an increase in the value of α tends to compress the induced streaming into a jet immediately adjacent to $\hat{y}=0$. Eq. (4.4) should be contrasted with the corresponding result for a laminar layer (Longuet-Higgins, 1953) where the maximum streaming velocity is $0.75\alpha+\mathrm{O}(\alpha^3)$.

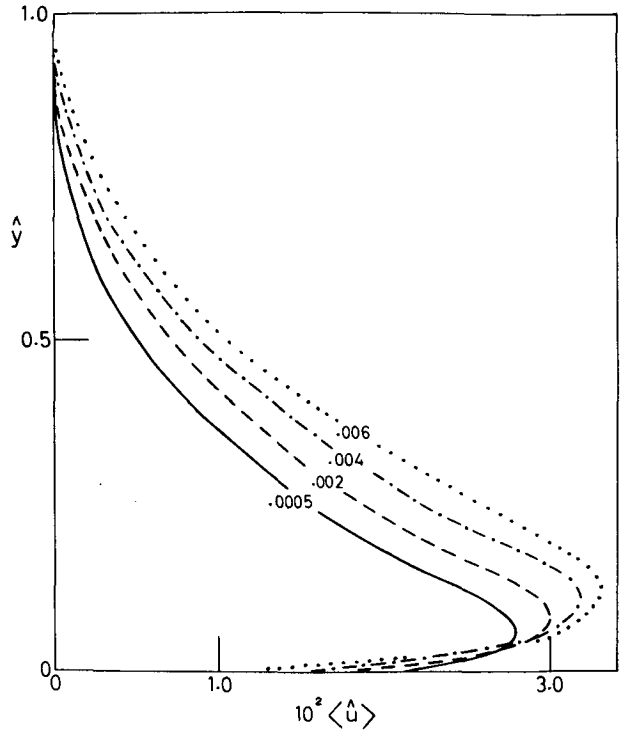

FIG. 2. As in Fig. 1 except $\alpha=0.1$; $5\times10^{-4}\leqslant\hat{y}_*\leqslant6\times10^{-3}$.

The second set of evaluations determines the effect of variations in the roughness length. With $\alpha=0.1$, we consider $5\times10^{-4}\leqslant\hat{y}_*\leqslant6\times10^{-3}$ and take $\hat{y}_0=0.02$ and $\hat{y}_1=1.0$. The resulting profiles of $\langle\hat{u}\rangle$ are shown in Fig. 2. The maximum value of $\langle\hat{u}\rangle$ is only weakly dependent upon $\hat{y}_*$ and again satisfies (4.4). However, the variation of $\langle\hat{u}\rangle$ with $\hat{y}_*$ is important at the outer edge of the logarithmic layer and a best fit to a linear law shows that the streaming velocity is then well represented by

$$\langle\hat{u}\rangle=0.022-1.425\hat{y}_*. \tag{4.5}$$

The dependence of the bottom stress τ_b on the roughness length of the boundary elements may be determined from

$$\tau_b=\left(K\rho\frac{\partial\bar{u}}{\partial y}\right)_{y=y_*}, \tag{4.6}$$

which yields

$$\frac{\tau_b}{\rho u_\infty{}^2}=c^{\frac{1}{2}}\hat{E}_0\,\mathrm{sgn}(\hat{u}_0), \tag{4.7}$$

where $\hat{E}_0$ and $\hat{u}_0$ refer to the values of $\hat{E}$ and $\hat{u}$ at $\hat{y}=0$. The variation of τ_b with the phase χ is given for various $\hat{y}_*$ in Fig. 3. It is clear that the bottom stress does not have a simple dependence on χ. Although the primary dependence of τ_b is on a harmonic involving $\cos\chi$, there is an important contribution from $\sin3\chi$ and it is not possible to represent τ_b by a simple empirical law. A frequently used representation of τ_b in terms of the orbital wave velocity just beyond the boundary layer has the form

$$\tau_b=C_f\rho|U|U, \tag{4.8}$$

which, using (2.3), leads to

$$\frac{\tau_b}{\rho u_\infty{}^2}=C_f|\cos\chi|\cos\chi, \tag{4.9}$$

where C_f is a friction coefficient. Eq. (4.9), however, does not reproduce the important contribution from $\sin3\chi$ and will not, therefore, accurately describe the detailed variation of the bottom stress given in Fig. 3. Nevertheless, a value for C_f can be derived that leads

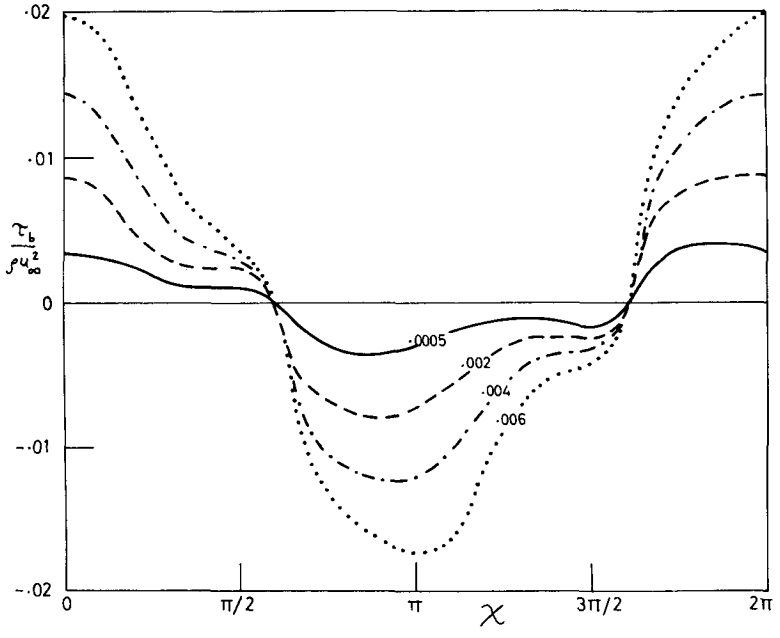

FIG. 3. Variation of bottom stress τ_b with phase χ: $\alpha=0.1$; $5\times10^{-4}\leqslant\hat{y}_*\leqslant6\times10^{-3}$.

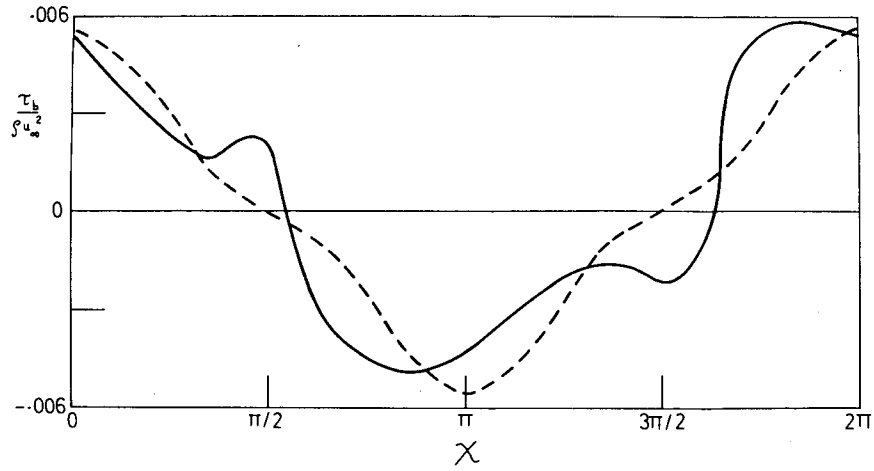

FIG. 4. As in Fig. 3 except $\alpha=0.1$, $\hat{y}_*=10^{-3}$. The solid line is the boundary layer calculation. The dashed line from Eq. (4.9) with $C_f=5.52\times10^{-3}$.

to the best approximation to the bottom stress by writing

$$C_f=\frac{\int_0^{2\pi}(\tau_b/\rho u_\infty^2)\,|\cos X|\cos X dX}{\int_0^{2\pi}\cos^4 X dX}. \tag{4.10}$$

Considering the case when $\alpha=0.1$, $\hat{y}_*=10^{-3}$, we find that $C_f\approx5.52\times10^{-3}$. The reconstruction of the bottom stress using this value of C_f in (4.9) is compared with the boundary layer evaluation in Fig. 4. Apart from the failure of (4.9) to produce the variation in τ_b resulting from $\sin 3X$, it will also be observed that (4.9) does not yield a nonzero component of mean bottom stress. In the present case, this mean value is given by

$$\frac{\langle\tau_b\rangle}{\rho u_\infty^2}=2.26\times10^{-5} \tag{4.11}$$

and has the same sense as the induced streaming motion.

The evaluation of the friction coefficient by Eq. (4.10) has been carried out for $\alpha=0.1$ and the range of roughness lengths considered earlier. The resulting values of C_f have been fitted by a least-squares method to a power law representation and we find that

$$C_f\approx0.74\hat{y}_*^{0.71} \tag{4.12}$$

with $5\times10^{-4}\leqslant\hat{y}_*\leqslant6\times10^{-3}$. Taking account of a different definition of the friction coefficient, a study by Kajiura (1968) suggests that $C_f=0.85\ (u_\infty/\sigma y_*)^{-\frac{2}{3}}$, which compares well with (4.12).

Again, considering the typical field data given in Section 4 and taking $\hat{y}_*=3\times10^{-3}$, the corresponding roughness length is ~0.9 mm. Eq. (4.12) then yields $C_f\approx1.2\times10^{-2}$. This agrees with typical values reported by Bretschneider (1954) in a field investigation of the energy loss of shallow water ocean waves.

In conclusion, it is appropriate to comment on the value selected for $\hat{y}_0$ in the numerical evaluations. As has been previously mentioned, the numerical process described in this paper becomes unstable for $\hat{y}_0\lesssim0.016$. This is almost certainly the result of the increasing strength of the singularity at $\hat{y}=0$ in Eqs. (3.3) and (3.4) as $\hat{y}_0\to0$. Nevertheless, it is important to know to what extent the results of this paper depend upon the nonzero numerical value used for $\hat{y}_0$. This point has been considered by comparing evaluations of the maximum steady streaming velocity and the bottom stress for values of $\hat{y}_0$ between 0.02 and 0.05. This comparison shows that the evaluations have only a weak dependence upon $\hat{y}_0$ at the lower end of the range of values considered. The results of this paper are not, therefore, thought to be significantly dependent upon the prescribed thickness of the logarithmic layer.

REFERENCES

Bretschneider, C. L., 1954: Field investigation of wave energy loss of shallow water ocean waves. U. S. Army, Beach Erosion Board, Tech. Memo. 46.

Carter, T. G., P. Lui and C. C. Mei, 1973: Mass transport by waves and offshore bedforms. *J. Waterways Harbors and Coastal Eng. Div. Proc. ASCE*, **99**, 165–184.

Collins, J. I., 1963: Inception of turbulence at the bed under periodic gravity waves. *J. Geophys. Res.*, **68**, 6007–6014.

Johns, B., 1970: On the mass transport induced by oscillatory flow in a turbulent boundary layer. *J. Fluid Mech.*, **43**, 177–185.

Jonsson, I. G., and N. A. Carlsen, 1976: Experimental and theoretical investigations in an oscillatory turbulent boundary layer. *J. Hydrol. Res.*, **14**, 45–59.

Kajiura, K., 1968: A model of the bottom boundary layer in waves. *Bull. Earthquake Res. Inst., Tokyo Univ.*, **46**, 75–123.

Launder, B. E., and D. B. Spalding, 1972: *Mathematical Models of Turbulence*. Academic Press, 169 pp.

Longuet-Higgins, M. S., 1953: Mass transport in water waves. *Phil. Trans. Roy. Soc. London*, **A245**, 535–581.

——, 1970: Longshore currents generated by obliquely incident sea waves, 1. *J. Geophys. Res.*, **75**, 6778–6789.

Russell, R. C. H., and J. D. C. Osorio, 1958: An experimental investigation of drift profiles in a closed channel. *Proc. 6th Conf. Coastal Eng.*, Miami, Council on Wave Research, University of California, 171–193.

Weatherly, G. L., 1975: A numerical study of time-dependent turbulent Ekman layers over horizontal and sloping bottoms. *J. Phys. Oceanogr.*, **5**, 288–299.